Single Quantum Dot Coupled to a Scanning Optical Antenna: A Tunable Superemitter

J. N. Farahani, D. W. Pohl, H.-J. Eisler, and B. Hecht*

Nano-Optics group, National Center of Competence for Research in Nanoscale Science, Institute of Physics, University of Basel, Klingelbergstr. 82, CH-4056 Basel, Switzerland

(Received 30 December 2004; published 28 June 2005)

The interaction of a single quantum dot with a bowtie antenna is demonstrated for visible light. The antenna is generated at the apex of a Si_3N_4 atomic force microscopy tip by focused ion beam milling. When scanned over the quantum dot, its photoluminescence is enhanced while its excited-state lifetime is decreased. Our observations demonstrate that the relaxation channels of a single quantum emitter can be controlled by coupling to an efficiently radiating metallic nanoantenna.

DOI: 10.1103/PhysRevLett.95.017402 PACS numbers: 78.67.Hc, 07.79.Fc, 33.70.Ca, 84.40.Ba

Control and optimization of the radiative properties of single quantum emitters is a core issue of present day optical science and technology. Such control capability may have impact, e.g., on surface-enhanced Raman scattering (SERS) [1,2], quenching effects [3], quantum information technology [4,5], plasmonics [6,7], and scanning near-field optical microscopy [8,9].

The proximity of a quantum emitter to a metal structure results in energy transfer to density fluctuations of the free electron gas. The associated currents generate radiation fields outside the structure and Ohmic losses inside. Depending on the relative weight of the two effects, the radiation intensity of the coupled system is enhanced or decreased. Electromagnetic reciprocity [10] requires that the absorption cross section undergoes the same change if the emitter can be considered a two-level system.

Both radiation and Ohmic losses depend on the shape, size, and material of a metallic structure as well as on its position with respect to the quantum emitter. Absorption and scattering efficiency of a small particle, for instance, vary differently with volume [11], resulting in a dominance of Ohmic losses and quenching both for very small [12], as well as for very large particles (in the extreme a perfectly quenching metallic half-space [3]).

Structures designed to increase the radiation efficiency of a nanoscopic optical source consequently must be optimized with respect to size, shape, and material. In radio-wave technology, such optimized structures are known as *antennas*. Common radio-wave antennas, hence, may be a good starting point for the design and optimization of optical enhancement schemes [13]. A single quantum emitter, positioned inside the *subwavelength size feed gap* of such an antenna, couples to the antenna arms in a similar way as a radio-wave guiding device (and *vice versa*) [14]. Optimum coupling requires impedance matching between quantum emitter and antenna, the impedence of the latter depending on wavelength, here, of light. It should be noted, however, that *optimized* optical antennas may differ considerably from their radio-wave counterparts because the electric properties of metals are quite disparate in the two frequency regimes, resulting in a potential for resonant plasmon excitation in the optical regime, but also in increased damping due to Ohmic losses.

Field enhancement and confinement by antennas was demonstrated for the infrared and microwave regime in the past [15,16]. More recently, antennas at optical wavelengths have raised attention [17,18]. However, sharp elongated tips [8,9,19–24], small apertures [25], and small particles [2] have been mainly used to study field enhancement effects in the optical regime so far.

In this Letter we report on the interaction of an optical antenna with single quantum emitters and the resulting modification of their radiative properties. To this end, we studied the photoluminescence (PL) of single semiconductor nanocrystal quantum dots (NC) positioned at a variable distance from a miniaturized bowtie antenna. Specifically, a dominance of radiation enhancement over nonradiative losses was found when the antenna is centered above the NC and illuminated appropriately. The results open new perspectives for the advancement of high-resolution microscopy and spectroscopy, sensing, and quantum information technology.

For our single-particle experiments, $[CdSe]_{core}\{ZnS\}_{shell}$ colloidal NCs (diameter ≈ 10 nm) are dispersed onto clean glass coverslips and coated with $a \leq 10$ nm thickness layer of poly(methylmethacrylate) (PMMA) for fixation. The NC photoluminesce appears at 585 nm (2.12 eV) with a FWHM bandwidth of 25 nm at the ensemble level. Atomic force microscope (AFM) images show NCs as hardly visible elevations of the otherwise flat PMMA surface.

The sample is mounted on a sample-scanning confocal optical microscope based on an inverted microscope (Zeiss Axiovert 135) combined with a tip-scanning AFM (Veeco, Bioscope) operating in contact mode [26]. A linearly polarized pulsed laser (Time Bandwidth Products, GE-100, 10 ps pulse width, 80 MHz repetition rate, frequency doubled to $\lambda_0 = 532$ nm, pulse picked to 5 MHz) is used for excitation. After passing a single-mode optical fiber for spatial filtering, the light is collimated by a lens and reflected via a dichroic mirror onto the back aperture of an oil immersion objective (Zeiss, Plan-Apochromat, ×63,

1.4 numerical aperture, ∞) and focused to a diffraction-limited spot on the sample. Emission from the sample is collected by the same objective and transmitted through the dichroic mirror. The angular ranges of acceptance for absorption and emission therefore are the same. A set of cutoff and short pass filters (550–600 nm, transmission $\geq 60\%$) removes residual excitation light and the 675 nm line of the AFM deflection laser. The transmitted PL is focused onto the 200 μm diameter active area of a single-photon counting avalanche photodiode (SPAD) (SPCM-ARQ 13, Perkin-Elmer) which serves as confocal pinhole. The SPAD is connected to a time-correlated single-photon counting card (Timeharp 200, PicoQuant, Berlin). For each photon, the times elapsed until arrival of the next laser pulse, as well as since the start of the scan image, and since the start of the scan line, are recorded. This allows us to construct spatial maps of the PL count rate and of the excited-state lifetime. For the latter, at each pixel, the full PL decay histogram is available.

The antennas were fabricated at the apices of the pyramidal Si_3N_4 AFM cantilever tips (DNP, Digital Instruments). After evaporating a homogeneous 40 nm thickness aluminum film, a bowtie-shaped metallic structure was sculptured from the film by means of focused ion beam (FIB) milling. This includes, in a final step, cutting of a narrow gap between the two arms of the antenna right at the apex. Figure 1 shows top (a) and side view (b) scanning electron microscope (SEM) images of such a bowtie antenna. The FIB milling procedure affected also the Si_3N_4 substrate beneath the film such that the final metal structure is located on two Si_3N_4 pillars. The inset of Fig. 1(b) indicates a gap width between the bowtie arms not quite as small as it appears in the top view, Fig. 1(a). The antenna is rounded at the top and slightly tilted with respect to the axis of the pyramid. Flare angle, radius of curvature of the antenna arms at the feed gap, and feed gap width, determined from Figs. 1(a) and 1(b), are 40°, 30 nm, and ≈ 50 nm, respectively. The overall antenna length is 170 nm, which is in between the length of the half wave dipole, estimated to be near 120 nm under consideration of the average dielectric properties of the environment, and the first minimum of the antenna responsivity at about twice that length [14].

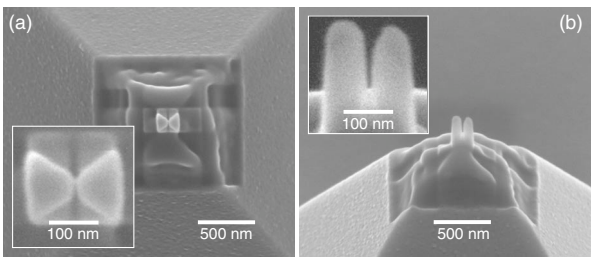

FIG. 1. Optical antenna at the apex of an AFM tip. (a) Top, (b) side view. Dimensions: aluminum thickness 40 nm; antenna overall length, 170 nm; flare angle, 40°; and feed gap width, ≈ 50 nm; radius of curvature at the feed gap, 30 nm.

The conditions for NC excitation in the linear regime were carefully determined. Saturation intensity and absorption cross section, σ_0, averaged over 87 individual NCs, were found to be 14 $\mu W/\mu m^2$ and 9×10^{-16} cm^2, respectively, in good agreement with Ref. [27]. All experimental data discussed below were obtained at excitation levels (~ 200 nW) far below the saturation level.

To investigate the coupling to the antenna structure, a single NC was centered and kept fixed in the laser focus. For this purpose, the sample positioning stage was adjusted for maximum PL count rate. Next, the optical antenna probe was raster scanned in the x and y direction (fast and slow axis, respectively) over a 2×2 μm^2 area across the NC, respectively, the focus. During scanning, the antenna arm on the slightly longer pillar is in physical contact with the soft polymer film. Count rate $R(x, y)$ and excited-state lifetime $\tau(x, y)$ maps were recorded for polarizations (white arrows) parallel [Figs. 2(a)–2(c)] and perpendicular to the long axis of the bowtie antenna [Figs. 2(d)–2(f)]. The insets on the left show, to scale, SEM images of the antenna probe. The measurement was repeated with a number of antenna probes that yielded similar results. For control and comparison, the same types of images were also recorded with a fully Al-coated probe tip [Figs. 2(g)–2(i)].

The count rate and excited-state lifetime fluctuate during image acquisition (blinking) [28]. For image analysis, we selected records which show an unperturbed count rate well in between maximum and minimum values in the

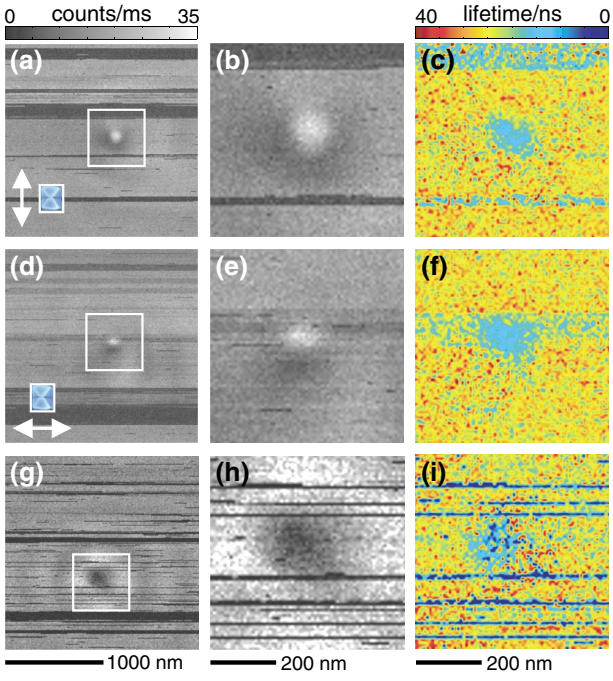

FIG. 2 (color). PL count rates (a),(b),(d),(e),(g),(h) and single exciton lifetimes (c),(f),(i) vs antenna position. (a)–(c) parallel; (d)–(f) perpendicular polarization; (g)–(i) fully coated tip. Center and left columns are zooms from the marked areas on the left. Insets: Antennas, to scale.

range of y values where the antenna passes (in the x direction) right over the NC (count rate ≈ 15 counts/ms, excited-state lifetime ≈ 26 ns). The antenna probe generates a pronounced *single maximum* of the count rate ($\approx$35 counts/ms) when centered above the NC, accompanied by a strong reduction in the excited-state lifetime [Figs. 2(a)–2(f)]. This is in contrast to the PL quenching observed with the fully coated tip [Figs. 2(g)–2(i)] [26] at the same position. It also differs qualitatively from the *pairs* of enhancement regions with a dark spot in between produced by very sharp elongated metal tips [24]. The maximum PL intensities are about the same for both polarizations but the excited-state lifetimes at the respective positions differ considerably (perpendicular: 10 ns; parallel 15 ns). Off center, the count rate images show regions with lower rates which are not obvious in the lifetime images. The asymmetry of these regions is probably caused by the uneven height of the antenna arms (Fig. 1).

The PL count rate and the lifetime can be written as

$$R = \xi\eta\sigma I, \qquad \tau = (k_r + k_{nr})^{-1} \tag{1}$$

where I is the time-averaged excitation photon flux density at the position of the NC without antenna. ξ, k_r, k_{nr}, $\eta = k_r/(k_r + k_{nr})$, and σ are the PL detection efficiency, radiative and nonradiative decay rates, PL quantum yield, and absorption cross section, respectively, all depending on the tip position (x, y). As a reference for the unperturbed NC, we define R_0 and τ_0 as averages over all pixels outside the NC/antenna interaction range with $R > 90\%$ of the maximum emission [28]. The maximum count rates of the unperturbed NCs correspond to an unperturbed quantum yield $\eta_0 \approx 1$ [28,29], in perfect agreement with the saturation data mentioned above.

Under the influence of the antenna probe, the effective cross section becomes $\sigma(x, y) = |\alpha(x, y)|^2\sigma_0$, where $\alpha(x, y)$ is the field enhancement factor defined as ratio of the projections of the electric field at the position of the NC onto the dipole moment with and without antenna. We introduce the normalized count rate

$$\gamma(x, y) = R(x, y)/R_0 = \eta(x, y)|\alpha(x, y)|^2 \tag{2}$$

and the normalized excited-state lifetime

$$\theta(x, y) = \tau(x, y)/\tau_0. \tag{3}$$

For further discussion, we treat the NC as an effective two-level system. Even under consideration of the frequency dependent responsivity of the dipole antenna, the enhancement factor of the antenna will not differ considerably for excitation and emission frequencies. Hence, and under consideration of the reciprocity theorem of optics [10], we may write [30,31]

$$\sigma/\sigma_0 = k_r/k_{r,0} = |\alpha(x, y)|^2. \tag{4}$$

We now calculate the product and ratio of the normalized count rate and lifetime to obtain

$$\gamma(x, y)\theta(x, y) = \eta^2(x, y), \tag{5}$$

$$\gamma(x, y)/\theta(x, y) = k_r^2(x, y)/k_{r,0}^2, \tag{6}$$

from which $\eta(x, y)$, $k_r(x, y)$, and evidently also

$$k_{nr}(x, y) = [1/\eta(x, y) - 1]k_r(x, y) \tag{7}$$

can be readily determined.

The corresponding maps are shown in Fig. 3 for parallel [3(a)–3(c)] and perpendicular polarization [3(d)–3(f)] for the antenna probe, and for the fully coated tip [3(g)–3(i)].

The antenna exhibits a distinct localized maximum in k_r for both polarizations that also represents a maximum of σ and of $|\alpha(x, y)|^2$ according to Eq. (4). For the fully coated tip, however, $|\alpha|^2$ turns out to be minimal beneath the tip apex, in agreement with expectation for the chosen illumination geometry [21,32].

The regions of increased and reduced PL quantum yield and of nonradiative decay rate resemble each other in shape, in particular, in regions of small k_{nr}, as to be expected from the definition of η. The increase of k_{nr} and the concomitant decrease of η outside the central spot indicate a prevalence of nonradiative relaxation pathways when the NC is right beneath one of the antenna arms. The effect is so pronounced for perpendicular polarization [compare Figs. 3(c) and 3(f)] that a remarkable reduction of the central spot size along the bowtie direction results [Figs. 3(b) and 3(e)].

The extreme values of η and k_{nr} do not coincide with those of k_r for the antenna probe. The differences demonstrate that radiative (field enhancement) and nonradiative

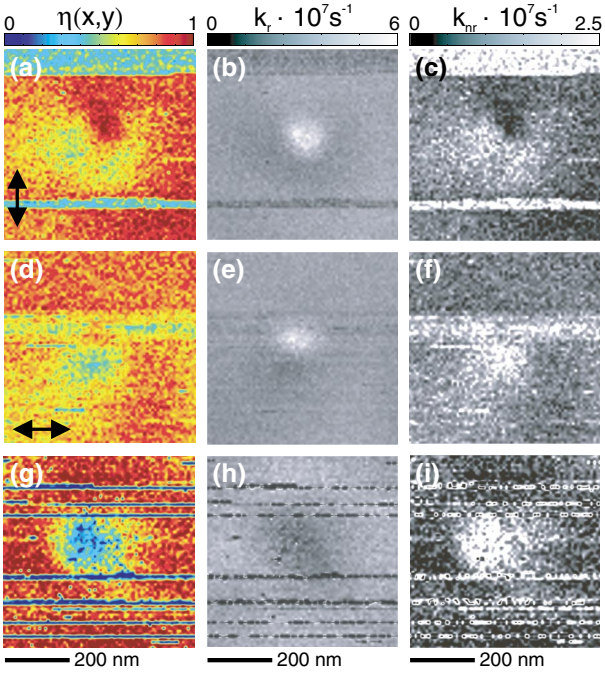

FIG. 3 (color). Maps of $\eta(x, y)$ (left column), $k_r(x, y)$ (center column), and $k_{nr}(x, y)$ (right column). Note that $\sigma \sim |\alpha(x, y)|^2 \sim k_r(x, y)$.

relaxation channels are independent from each other in the first place, although both become prominent close to the metal structure. Again, the observed asymmetric patterns may be related to the asymmetric tip shape.

It is particularly remarkable that for parallel (perpendicular) polarization, η increases from the momentary unperturbed value of $\sim 0.8(0.65)$ at both ends of the scan lines to $\sim 1(0.8)$ in the presence of the antenna which is a clear demonstration of an antenna effect: Observed from outside, the NC/antenna system is indistinguishable from an *effective* quantum emitter, i.e., a "*superemitter*," with widely adjustable photophysical parameters. Another surprising finding is the nearly complete quenching of the *nonradiative* decay rate seen in the center of Fig. 3(c). It indicates an influence of the antenna on the *internal* nonradiative decay channels of the NC by a not yet identified mechanism. We speculate that physical contact between the antenna and nanocrystal changes the distribution and/or barrier heights of trap states outside the nanocrystal.

Quite generally, the present experiment demonstrates quantitatively the tunability of radiative and nonradiative decay rates of single quantum emitters by the proximity of a suitable metal nanostructure. The results obtained show that this is not only achieved by enhanced excitation due to local fields. Obviously, the other relevant parameter is the emission efficiency of the metal structure, its *radiation resistances* in the language of antenna theory.

The absorption and emission properties of a superemitter can be optimized by the appropriate combination of quantum emitters and miniaturized antennas. The quantum emitter part can be tailored to link to the molecular world which is of particular relevance in biology; it also can act as a converter of electrical into optical energy or of optical waves with different frequencies via real (fluorescence, PL) or virtual transitions (Raman effect, parametric processes). The antenna part can be tailored to provide absorption or emission at certain favored frequencies, into chosen directions, with prescribed polarization. The respective absorption cross section of the superemitter and its radiative transition rate can be enormously increased. The feed gap can be shaped for optimum coupling to dipolar quantum emitters, but could also be adapted to higher-order multipole transitions.

Positioning of the antenna with respect to the quantum emitters was facilitated in the present experiment by the use of an AFM. Superemitters, however, might also be formed by other methods and in a more permanent way, for instance by self-assembly. Superemitters hence can be of interest for various fields of science, ranging from pure spectroscopy to biological microscopy, microoptoelectronics, and quantum information technology, just to name a few.

The authors gratefully acknowledge continuous support by H. J. Güntherodt and Ch. Schönenberger, many helpful discussions with A. Lieb, P. Mühlschlegel, J. Toquant, S. Karotke, J. Y. P. Butter, Y. Lill, O. J. F. Martin, and L. Novotny, as well as financial support from the Swiss National Science Foundation via the National Center of Competence in Research (NCCR) in Nanoscale Science and a professorship for one of the authors (B. H.).

*Electronic address: bert.hect@nano-optics.ch

[1] K. Kneipp *et al.*, Phys. Rev. Lett. **78**, 1667 (1997).
[2] J. Jackson *et al.*, Appl. Phys. Lett. **82**, 257 (2003).
[3] R. R. Chance, A. Prock, and R. Silbey, Adv. Chem. Phys. **60**, 1 (1978).
[4] B. Lounis and W. E. Moerner, Nature (London) **407**, 491 (2000).
[5] P. Michler *et al.*, Science **290**, 2282 (2000).
[6] H. Ditlbacher *et al.*, Appl. Phys. Lett. **80**, 404 (2002).
[7] S. Bozhevolnyi *et al.*, Phys. Rev. Lett. **86**, 3008 (2001).
[8] A. Hartschuh, E. Sánchez, X. Xie, and L. Novotny, Phys. Rev. Lett. **90**, 095503 (2003).
[9] T. Ichimura *et al.*, Phys. Rev. Lett. **92**, 220801 (2004).
[10] R. Carminati, M. Nieto-Vesperinas, and J.-J. Greffet, J. Opt. Soc. Am. A **15**, 706 (1998).
[11] G. Mie, Ann. Phys. (Berlin) **25**, 377 (1908).
[12] E. Dulkeith *et al.*, Phys. Rev. Lett. **89**, 203002 (2002).
[13] D. Pohl, in *Near-Field Optics: Principles and Applications*, edited by M. Ohtsu and X. Zhu (World Scientific, Singapore, 2000), ISBN 981-02-4365-0, p. 9.
[14] C. Balanis, *Antenna Theory: Analysis and Design* (John Wiley & Sons, New York, Chichester, 1997), 2nd ed.
[15] R. Grober, R. Schoellkopf, and D. Prober, Appl. Phys. Lett. **70**, 1354 (1997).
[16] B. Knoll and F. Keilmann, Nature (London) **399**, 134 (1999).
[17] K. Crozier, A. Sundaramurthy, G. Kino, and C. Quate, J. Appl. Phys. **94**, 4632 (2003).
[18] D. Fromm *et al.*, Nano Lett. **4**, 957 (2004).
[19] W. Denk and D. W. Pohl, J. Vac. Sci. Technol. B **9**, 510 (1991).
[20] C. Girard, O. Martin, and A. Dereux, Phys. Rev. Lett. **75**, 3098 (1995).
[21] L. Novotny, R. X. Bian, and X. S. Xie, Phys. Rev. Lett. **79**, 645 (1997).
[22] R. Stöckle, Y. Suh, V. Deckert, and R. Zenobi, Chem. Phys. Lett. **318**, 131 (2000).
[23] J. Gerton *et al.*, Phys. Rev. Lett. **93**, 180801 (2004).
[24] H. Frey, S. Witt, K. Felderer, and R. Guckenberger, Phys. Rev. Lett. **93**, 200801 (2004).
[25] H. Gersen *et al.*, Phys. Rev. Lett. **85**, 5312 (2000).
[26] W. Trabesinger *et al.*, Appl. Phys. Lett. **81**, 2118 (2002).
[27] C. Leatherdale, W.-K. Woo, F. Mikulec, and M. Bawendi, J. Phys. Chem. B **106**, 7619 (2002).
[28] B. Fisher, H.-J. Eisler, N. Stott, and M. Bawendi, J. Phys. Chem. B **108**, 143 (2004).
[29] X. Brokmann, L. Coolen, M. Dahan, and J. Hermier, Phys. Rev. Lett. **93**, 107403 (2004).
[30] J. Azoulay, A. Débarre, A. Richard, and P. Tchénio, Europhys. Lett. **51**, 374 (2000).
[31] K. Shimizu *et al.*, Phys. Rev. Lett. **89**, 117401 (2002).
[32] M. Thomas, J.-J. Greffet, R. Carminati, and J. R. Arias-Gonzalez, Appl. Phys. Lett. **85**, 3863 (2004).